Available online at www.sciencedirect.com
ScienceDirect
Journal of Sound and Vibration 310 (2008) 608–630
JOURNAL OF SOUND AND VIBRATION
www.elsevier.com/locate/jsvi

Prediction of vibrations induced by underground railway traffic in Beijing

S. Gupta[a,*], W.F. Liu[b], G. Degrande[a], G. Lombaert[a], W.N. Liu[b]

[a]*Department of Civil Engineering, K.U. Leuven, Kasteelpark Arenberg 40, B-3001 Leuven, Belgium*
[b]*Department of Tunnelling and Geotechnical Engineering, Beijing Jiaotong University, Xizhimenwai, Beijing 100044, China*

Accepted 13 July 2007
The peer review of this article was organised by the Guest Editor
Available online 20 August 2007

Abstract

This paper examines the problem of subway induced vibrations on line 4 of Beijing metro, which is currently under construction and is planned to pass in close proximity of the Physics Laboratory of Beijing University. The laboratory has a lot of equipment that is very sensitive to traffic induced vibrations and future operation of metro line 4 is a matter of concern. Hence, it is important to study the influence of subway induced vibrations inside the laboratory and to propose a viable solution to mitigate the vibrations. In this paper, the tunnel north of Chengfulu station is modelled using a coupled periodic FE–BE model and the free-field response due to moving trains is predicted. In addition, vibration measurements have been performed on the site of the Physics Laboratory to estimate the existing vibration levels due to road traffic. The predicted and measured vibrations are superimposed to assess the vibrations due to the combined effect of road and railway traffic in the vicinity of the Physics Laboratory. Apart from the numerical investigations, vibration measurements have also been performed on a similar site at line 1 of Beijing metro to substantiate the estimated results on metro line 4. Finally, it is studied how the vibrations can be controlled using a floating slab track, which is widely used as an effective measure of vibration isolation in tunnels. The efficiency of a 7.9 Hz floating slab track as a vibration countermeasure is assessed in this paper. This study demonstrates the applicability of the numerical model for the relevant assessment of subway induced vibrations and its use to study the performance of different track structures in the tunnel.

1. Introduction

Vibrations induced by the passage of underground trains are a major environmental concern in urban areas. These vibrations propagate through the tunnel and surrounding soil into nearby buildings causing annoyance to people. Vibrations may also interfere with sensitive equipment, as used in scientific research laboratories and hightech industries.

This paper examines the problem of subway induced vibrations in Beijing. Beijing metro is a rapid transit system that serves Beijing city and its various outlying suburbs. There are ambitious plans to expand the subway network in the Chinese capital, which include both subway, light rail and suburban trains. One of the

*Corresponding author. Tel.: +32 16 32 16 77; fax: +32 16 32 19 88.
E-mail address: shashank.gupta@bwk.kuleuven.be (S. Gupta).

0022-460X/$ - see front matter © 2007 Elsevier Ltd. All rights reserved.
doi:10.1016/j.jsv.2007.07.016

projects currently under construction is metro line 4 which is planned in close proximity of the Physics Laboratory of Beijing University, where a lot of sensitive equipment is used that could be affected by subway induced vibrations. It is therefore important to study the influence of subway induced vibrations and to propose a solution to mitigate the vibrations.

Vibration measurements have been performed on the site of the Physics Laboratory of Beijing University to determine the existing vibration levels due to road traffic. A brief account of these vibration measurements is presented in Section 2. The background vibration levels are compared to the mechanical vibration specification of an electron microscope present inside the laboratory.

Apart from the road traffic, the future operation of metro line 4 can impair the operating conditions of the sensitive equipment inside the Physics Laboratory. In order to reduce the vibration and noise disturbance, some studies based on in situ measurements and numerical analysis have been proposed. As far as numerical modelling is concerned, two-dimensional [1–3] and three-dimensional modelling [4–6] based on the finite element (FE) method, the boundary element (BE) method or the coupled FE–BE method [7,8] have been developed in the past.

In this paper, a coupled periodic FE–BE model [9–11] is used to analyze the dynamic response of a single bored concrete segmented tunnel on line 4 of Beijing metro, north of Chengfulu station. Section 3 presents the application of the numerical model, where the free-field vibrations due to a moving train on metro line 4 are predicted. The predicted vibrations from railway traffic are superimposed with the measured vibrations from the road traffic and the combined effect of road and railway traffic is studied. These results are analyzed in one-third octave bands and compared to the mechanical vibration specification of an electron microscope installed in the laboratory. This facilitates to study the influence of the future operation of metro line 4 on the vibrations inside the Physics Laboratory.

In addition, some vibration measurements have been performed on line 1 of Beijing metro during the passage of trains inside the tunnel. This site closely resembles the site north of Chengfulu station on line 4 of Beijing metro. Therefore, these vibration measurements give a good indication of the vibrations that could appear on the site of the Physics Laboratory of Beijing University due to future operation of metro line 4, if a similar track system is installed in the tunnel. These results are used to corroborate the findings of the numerical study on line 4 of Beijing metro. However, it should be mentioned that this is not an experimental validation of the numerical model, but only an illustration to demonstrate that the numerical predictions are realistic. Section 4 presents some important observations of this vibration measurement campaign.

In Section 5, an example of vibration mitigation using a floating slab track is presented. A floating slab track is widely used as an effective measure of vibration isolation in tunnels. The vibration isolation efficiency of the floating slab track is studied using the coupled periodic FE–BE model. The paper demonstrates how the vibration isolation efficiency of such a system can efficiently be studied using a state-of-the-art three-dimensional model.

2. Problem outline

Line 4 of the Beijing metro is currently under construction. When completed in 2008, it will be one of the main north–south underground lines in Beijing with a length of 29 km. North of Chengfulu station, line 4 passes at close proximity of the Physics Laboratory of Beijing University (Fig. 1), where a lot of sensitive equipment, including electron microscopes and a scanning tunnelling microscope is present. This equipment is very sensitive to traffic induced vibrations; apart from road traffic induced vibrations, the future operation of metro line 4 is a matter of concern. Excessive mechanical vibrations seriously affect the performance of a microscope and it is important when choosing a site to ensure that this type of interference is not present.

A measurement campaign was conducted in December 2005 at the site of the Physics Laboratory of Beijing University in order to determine the existing background vibration level outside and inside the laboratory.

Fig. 2 shows the positions of the accelerometers on the free surface outside the Physics Laboratory. The measurement points are located along the wall of the laboratory at a distance of 24, 37, 53 and 76 m from the center of the road. The vertical acceleration is measured in all these points in the absence and presence of the traffic on the road.

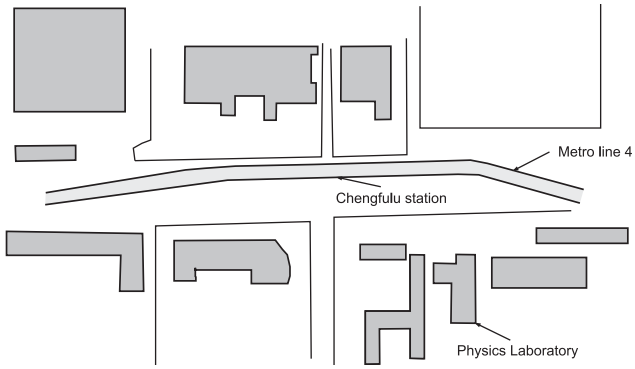

Fig. 1. Line 4 north of Chengfulu station.

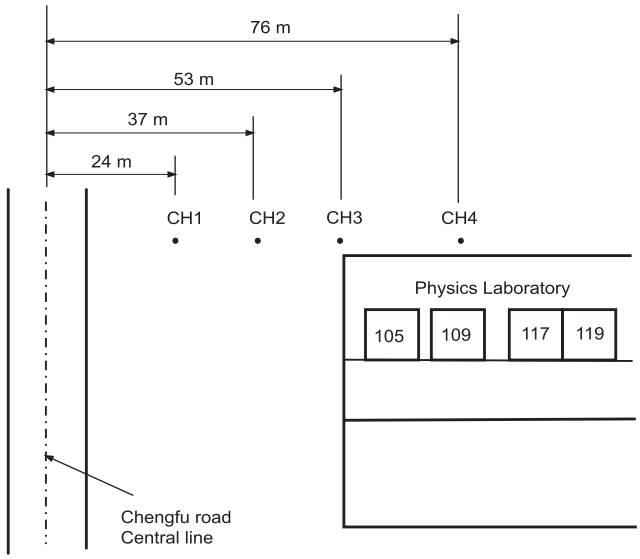

Fig. 2. Measurement points outside the Physics Laboratory.

Fig. 3 shows the one-third octave band RMS spectra of the vertical acceleration recorded at four measurement points without and with road traffic. Superimposed on this graph are the maximum allowable RMS values of the vertical acceleration for the Tecnai30 electron microscope. This mechanical vibration criterion is provided by the manufacturer of the Tecnai30 electron microscope and will be used as a representative criterion for the sensitive equipment inside the laboratory. According to the criterion the high-resolution performance will not be affected, if all frequency components are in zone I. If there are components which lie in zone II, the measurement results must be sent to the supply center service for further analysis, where it will be decided if the site is acceptable. If there are frequency components which lie in zone III, the site is unsuitable for installation.

The comparison of one-third octave band RMS spectra of the vertical acceleration measured in absence and presence of road traffic, clearly demonstrates the influence of the traffic on the road. There is an increase in the vertical acceleration in the low-frequency band between 8 and 30 Hz, which is the typical frequency range of interest for road traffic induced vibrations. Some frequency components lie in the zone II, which may be critical for the operation of sensitive instruments inside the laboratory.

In order to assess the operating conditions of the instruments in the Physics Laboratory, some vibration measurements have also been performed inside the laboratory.

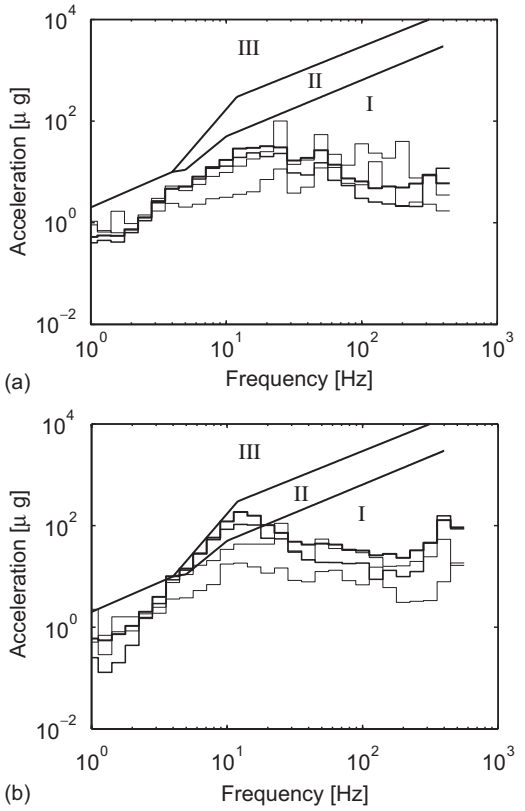

Fig. 3. One-third octave band RMS spectra of the vertical acceleration measured outside the Physics Laboratory (——— CH1, ——— CH2, ——— CH3, ——— CH4; decreasing line thickness) (a) without and (b) with traffic on the road. Superimposed on the graphs are the maximum allowable RMS values of the vertical acceleration for the Tecnai30 electron microscope.

Fig. 4 gives an overview of the accelerometers installed inside the laboratory. Four channels are measured by placing the accelerometers in the corridor, the doorway of room 119, on the floor of room 119 and on the isolated base of the microscope present in room 119. The foundation of the microscope is composed of a concrete block supported on resilient material that provides vibration isolation above 2 Hz.

Apart from studying the effect of road traffic, the influence of the disturbance caused by human activities inside the laboratory (footfall-induced vibrations in the corridor and the rooms) is also analyzed.

Fig. 5 shows the one-third octave band RMS spectra of the vertical acceleration at four measurement points inside the Physics Laboratory due to background sources and due to the excitation by people walking in the laboratory. The vibration levels inside room 119 are higher than in the corridor due to the presence of other vibratory sources close to this room in addition to the road traffic. It should be noted that the human activity inside the laboratory influences the floor vibration levels at all frequency components. The vibrations recorded on the floor of room 119 (CH3), during the disturbances from people, enter into zone III and II in the frequency range between 1 and 10 Hz and between 10 and 100 Hz, respectively. This can adversely affect the performance of the sensitive equipment.

The difference between the response measured on the floor of room 119 (CH3) and on the foundation of the electron microscope (CH4) is clearly seen from Fig. 5. The reduced response on the foundation demonstrates the efficiency of isolating the base of the electron microscope.

Most of the frequency components lie in zone I or II, which indicates proper operating conditions for the equipment at present. However, it should be noted that the vibration levels will increase due to the future operation of line 4 of Beijing metro and the RMS values may enter into zone III, which may hamper the performance of sensitive equipment. Therefore, the vibrations that will be generated from trains moving on metro line 4 are predicted and their influence is studied.

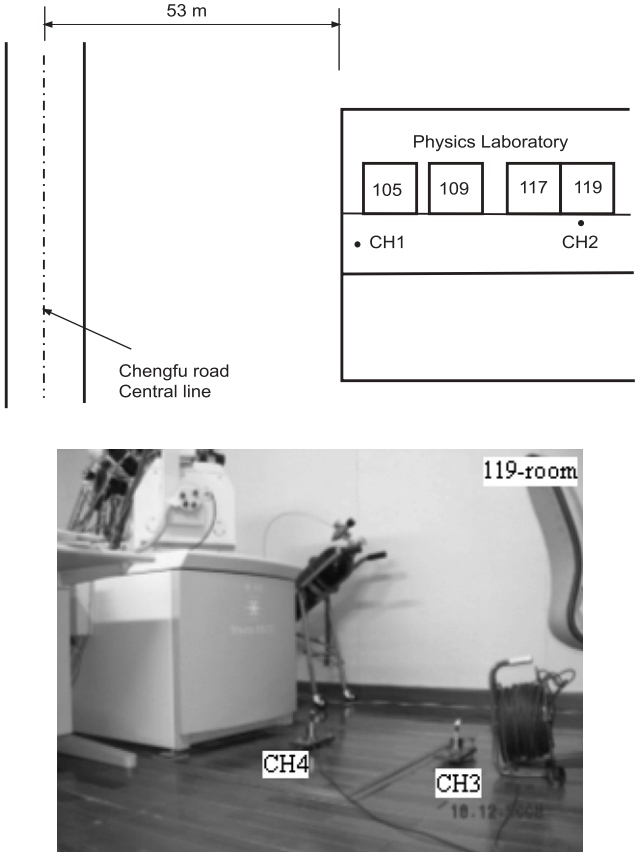

Fig. 4. Measurement points inside the Physics Laboratory for setup 1.

3. Numerical method

Within the frame of the EC-Growth project CONVURT [9], a coupled periodic FE–BE model has been developed that exploits the longitudinal invariance or periodicity of the track–tunnel–soil system [10,11]. The three-dimensional dynamic tunnel–soil interaction problem is solved with a subdomain formulation, using a finite element method for the tunnel and a boundary element method for the soil, modelled as a horizontally layered elastic half-space. The response to moving loads is deduced from the frequency content of the axle loads and the transfer functions in the frequency–wavenumber domain. The proposed numerical model accounts for the random excitation due to rail unevenness.

3.1. Response due to moving loads

In the fixed frame of reference, the distribution of n vertical axle loads moving in the longitudinal direction $\mathbf{e}_y$ on the coupled track–tunnel–soil system is written as the summation of the product of Dirac functions that determine the time-dependent position $\mathbf{x}_k = \{x_{k0}, y_{k0} + vt, z_{k0}\}^{\mathrm{T}}$ and the time history $g_k(t)$ of the kth axle load:

$$\rho\mathbf{b}(\mathbf{x}, t) = \sum_{k=1}^{n} \delta(x - x_{k0})\delta(y - y_{k0} - vt)\delta(z - z_{k0})g_k(t)\mathbf{e}_z \tag{1}$$

y_{k0} is the initial position of the kth axle that moves with the train speed v along the y-axis and $\mathbf{e}_z$ denotes the vertical unit vector.

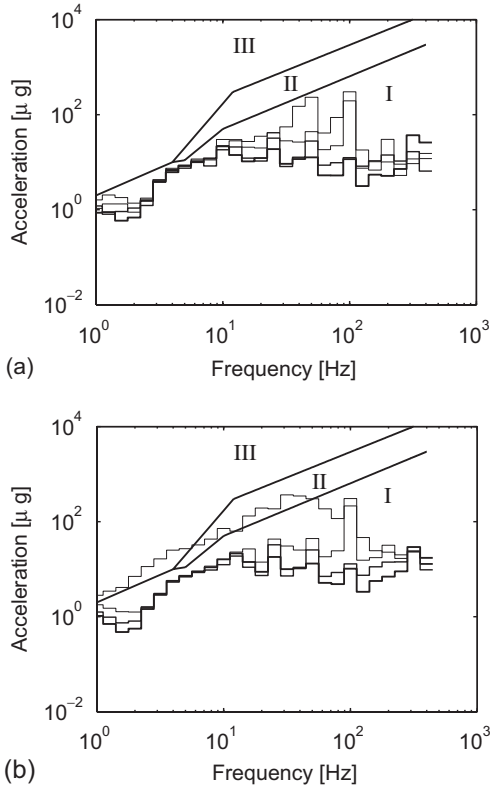

Fig. 5. One-third octave band RMS spectra of the vertical acceleration inside the Physics Laboratory (—— CH1, —— CH2, —— CH3, ——— CH4; decreasing line thickness) due to (a) background sources only and (b) disturbances from people inside the laboratory. Superimposed on the graphs are the maximum allowable RMS values of the vertical acceleration for the Tecnai30 electron microscope.

A Fourier transformation is applied to Eq. (1) to obtain the representation in the frequency–spatial domain:

$$\rho\hat{b}_j(\mathbf{x},\omega)=\frac{1}{v}\sum_{k=1}^{n} g_k\left(\frac{y-y_{k0}}{v}\right)\exp\left[-\mathrm{i}\frac{\omega}{v}(y-y_{k0})\right]\delta(x-x_{k0})\delta(z-z_{k0})\delta_{zj}. \tag{2}$$

The response in the frequency domain $\hat{u}_i(\mathbf{x},\omega)$ at the receiver point $\mathbf{x}$ due to n axle loads is written as the superposition of the load distribution along the source line:

$$\hat{u}_i(\mathbf{x},\omega)=\int_{-\infty}^{\infty}\rho\hat{b}_j(\mathbf{x}',\omega)\hat{h}_{ji}(\mathbf{x}',\mathbf{x},\omega)\,\mathrm{d}\mathbf{x}', \tag{3}$$

where $\hat{h}_{ji}(\mathbf{x}',\mathbf{x},\omega)$ is the transfer function, expressing the displacement at $\mathbf{x}$ in the $\mathbf{e}_i$ direction, due to a unit load applied at $\mathbf{x}'$ in the $\mathbf{e}_j$ direction. Substituting Eq. (2) in Eq. (3) and elaborating the dependency of the transfer function $\hat{h}_{ji}(\mathbf{x}',\mathbf{x},\omega)$ on the source coordinates gives:

$$\hat{u}_i(\mathbf{x},\omega)=\sum_{k=1}^{n}\int_{-\infty}^{\infty} g_k(\tau)\hat{h}_{zi}(x_{k0},y_{k0}+v\tau,z_{k0},\mathbf{x},\omega)\exp(-\mathrm{i}\omega\tau)\,\mathrm{d}\tau, \tag{4}$$

where $\tau=(y'-y_{k0})/v$.

The response due to a moving load on the track can therefore be calculated from the transfer functions of the track–tunnel–soil system describing the displacement at a point $\mathbf{x}$ due to a load at position $\mathbf{x}'$.

In case of an invariant or a periodic geometry, the expression (4) can be further simplified using the Fourier [12] or the Floquet transform [10,11].

An infinite periodic structure can be analyzed using the Floquet transform method by restricting the problem domain Ω to a single periodic unit $\tilde{\Omega}$ (the reference cell). If the spatial period is L, then the position $\mathbf{x}$

of any point in the problem domain is decomposed as $\mathbf{x} = \tilde{\mathbf{x}} + nL\mathbf{e}_y$, where $\tilde{\mathbf{x}}$ is the position in the reference cell and n is the cell number. The response to moving loads in case of periodic domains is given by [13,14]:

$$\hat{u}_i(\tilde{\mathbf{x}} + n_y L\mathbf{e}_y, \omega) = \frac{1}{2\pi}\sum_{k=1}^{n}\int_{-\infty}^{\infty}\hat{g}_k(\omega - k_y v)\exp[-\mathrm{i}k_y(n_y L - y_{k0})] \times \int_{-L/2}^{L/2}\exp(-\mathrm{i}k_y\tilde{y}_k)\tilde{\hat{h}}_{zi}(\tilde{\mathbf{x}}', \tilde{\mathbf{x}}, \kappa_y, \omega)\,\mathrm{d}\tilde{y}'\,\mathrm{d}k_y, \tag{5}$$

where $\kappa_y = k_y - 2m\pi/L$ and $k_y = (\omega - \tilde{\omega})/v$. The transfer function in the frequency–wavenumber domain $\tilde{\hat{h}}_{zi}(\tilde{\mathbf{x}}', \tilde{\mathbf{x}}, \kappa_y, \omega)$ is the Floquet transform of the transfer function in the frequency–spatial domain $\hat{h}_{zi}(\tilde{\mathbf{x}}', \tilde{\mathbf{x}} + n_y L\mathbf{e}_y, \omega)$.

It can be seen from Eq. (5) that the transfer function $\tilde{\hat{h}}_{zi}(\tilde{\mathbf{x}}', \tilde{\mathbf{x}}, \kappa_y, \omega)$ and the frequency content of the axle load $\hat{g}_k(\omega)$ are needed to compute the response to moving loads.

3.2. Transfer functions

The transfer functions are computed using the coupled periodic FE–BE model based on the classical domain decomposition approach, where the finite element method is used for the tunnel and the boundary element method is used for the soil. The Floquet transform is used to exploit the periodicity of geometry and to restrict the problem domain to a single bounded reference cell.

The tunnels north of Chengfulu station are two parallel bored tunnels with a segmented concrete lining at a depth of 13.5 m below the free surface. The distance between the tunnels is 13 m and both tunnels have an internal radius $r_i = 2.7$ m and a wall thickness $t = 0.3$ m. As shown in Fig. 6, the tunnel lining is composed of six circumferential segments for each ring, which are connected by bolts in the circumferential and longitudinal direction of the tunnel. The concrete lining has a Young's modulus $E^t = 35,000$ MPa, a Poisson's ratio $v^t = 0.25$, a density $\rho^t = 2500\,\mathrm{kg/m^3}$ and a hysteretic material damping ratio $\beta^t = 0.02$. A concrete slab is poured on the tunnel invert, with a Young's modulus $E^t = 28,500$ MPa, a Poisson's ratio $v^t = 0.2$, a density $\rho^t = 2500\,\mathrm{kg/m^3}$ and a hysteretic material damping ratio $\beta^t = 0.02$. In this paper, one tunnel north of

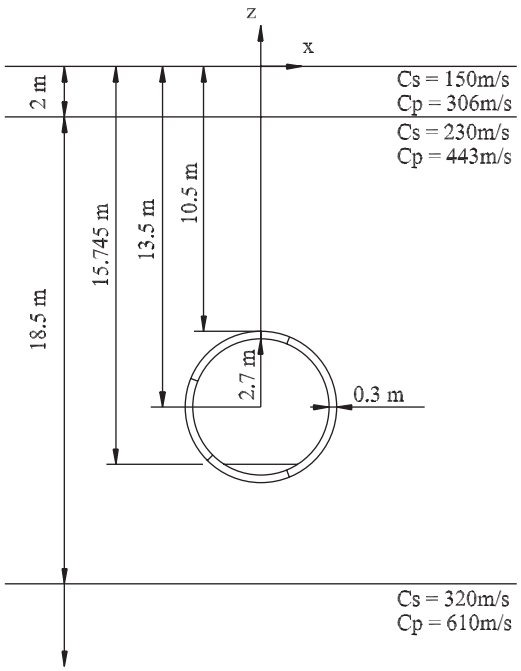

Fig. 6. Cross section of the tunnel on line 4, north of Chengfulu station.

Chengfulu station is modelled using the coupled periodic FE–BE model. The tunnel is considered invariant in the longitudinal direction and modelled as a periodic structure with spatial period $L = 0.6\,\mathrm{m}$.

The geological map of the area north of Chengfulu station shows that there are mainly three layers of soil: fill material, silty clay, gravel and pebble. The dynamic soil characteristics are summarized in Table 1. The tunnel is assumed to be embedded in a layered half-space consisting of a shallow layer of fill material (thickness $d = 2.0\,\mathrm{m}$) and a layer of silty clay ($d = 18.5\,\mathrm{m}$) on top of a homogeneous half-space consisting of a stiffer layer with gravel and pebble.

On line 4 of Beijing metro, T-60 rails will be used that have a cross-sectional area $A_r = 7.725 \times 10^{-3}\,\mathrm{m}^2$, a moment of inertia $I_r = 3.217 \times 10^{-5}\,\mathrm{m}^4$, a mass per unit length $\rho_r A_r = 60.64\,\mathrm{kg/m}$ and a bending stiffness $E_r I_r = 6.434 \times 10^6\,\mathrm{Nm}^2$. Soft rail pads with a stiffness $k_{\mathrm{rp}} = 50\,\mathrm{MN/m}$ discretely support the rails at an interval $d = 0.6\,\mathrm{m}$ on the sleepers. The concrete sleeper has a mass $M_s = 200\,\mathrm{kg}$. The track is modelled as an infinite beam on continuous support. The model consists of an infinite Euler beam, representing the (two) rails and the mass elements representing the sleepers. The mass of the sleepers is distributed in the longitudinal direction with a mass per unit length $m_s = M_s/d = 333\,\mathrm{kg/m}$. The rail pads are modelled as a continuous support with vertical stiffness $\bar{k}_{\mathrm{rp}} = k_{\mathrm{rp}}/d = 83.3\,\mathrm{MN/m}^2$ between the beam and the sleepers, while the rigid connection between the sleepers and the concrete slab is modelled with very stiff springs below the mass elements.

As the reference cell of the tunnel is bounded, the displacement field $\tilde{\mathbf{u}}_t(\tilde{\mathbf{x}}, \kappa_y, \omega)$ in the tunnel is decomposed on a basis of functions $\tilde{\boldsymbol{\psi}}_m(\tilde{\mathbf{x}}, \kappa_y)$:

$$\tilde{\mathbf{u}}_t(\tilde{\mathbf{x}}, \kappa_y, \omega) = \sum_{m=1}^{N} \tilde{\boldsymbol{\psi}}_m(\tilde{\mathbf{x}}, \kappa_y)\alpha_m(\kappa_y, \omega), \tag{6}$$

where $\tilde{\boldsymbol{\psi}}_m(\tilde{\mathbf{x}}, \kappa_y)$ is the kinematical basis that obeys the periodicity condition of the second kind [10,11].

The soil displacements $\tilde{\mathbf{u}}_s(\tilde{\mathbf{x}}, \kappa_y, \omega)$ can be written as the superposition of waves that are radiated by the tunnel into the soil:

$$\tilde{\mathbf{u}}_s(\tilde{\mathbf{x}}, \kappa_y, \omega) = \tilde{\mathbf{u}}_{\mathrm{sc}}(\tilde{\mathbf{u}}_t)(\tilde{\mathbf{x}}, \kappa_y, \omega) = \sum_{m=1}^{M} \tilde{\mathbf{u}}_{\mathrm{sc}}(\tilde{\boldsymbol{\psi}}_m)(\tilde{\mathbf{x}}, \kappa_y, \omega)\alpha_m(\kappa_y, \omega). \tag{7}$$

The weak or variational formulation of the problem results in a dynamic tunnel–soil interaction equation in the frequency–wavenumber domain [10,11,15,16]:

$$[\mathbf{K}_t(\kappa_y) - \omega^2\mathbf{M}_t(\kappa_y) + \mathbf{K}_s(\kappa_y, \omega)]\boldsymbol{\alpha}(\kappa_y, \omega) = \mathbf{F}_t(\kappa_y, \omega), \tag{8}$$

where $\mathbf{K}_t(\kappa_y)$ and $\mathbf{M}_t(\kappa_y)$ are the dynamic stiffness and mass matrix of the tunnel, respectively. $\mathbf{K}_s(\kappa_y, \omega)$ is the dynamic stiffness matrix of the soil calculated with a periodic boundary element formulation with Green–Floquet functions defined on the periodic structure with period L along the tunnel [10,15–17]. This approach has the advantage that the existing three-dimensional BE technology for layered media can be reused, as the periodic Green's kernels have the same singularities as the three-dimensional Green's kernels [10,16]. Therefore, the proposed approach is also preferred for the analysis of translational invariant tunnels. A so-called 2.5D approach could also have been used, but would have necessitated the analysis of the singularities of the 2.5D Green's functions, which is now avoided by using the Green–Floquet functions.

The Craig–Bampton substructuring technique [18] is used to efficiently incorporate a track in the tunnel, describing the kinematics of the track-tunnel system as a superposition of the track modes on a rigid base and

Table 1
Dynamic soil characteristics on line 4, north of Chengfulu station

Layer	Soil type	d (m)	C_s (m/s)	C_p (m/s)	E ($\times 10^6\,\mathrm{N/m}^2$)	ν (dimensionless)	ρ ($\mathrm{kg/m}^3$)	β (dimensionless)
1	Fill material	2.0	150	306	116.6	0.341	1900	0.05
2	Silty clay	18.5	230	443	289.0	0.313	2023	0.04
3	Gravel and pebble	∞	320	610	704.0	0.223	1963	0.03

the quasi-static transmission of the free tunnel modes into the track [11]. Fig. 7 shows two free tunnel modes and a track mode on a rigid base computed at zero wavenumber. These periodic modes of the first kind are modified to obtain the periodic modes $\tilde{\boldsymbol{\psi}}_m(\tilde{\mathbf{x}}, \kappa_y)$ of the second kind [11]. Seventy-two periodic modes of the second kind are used for the computation at each wavenumber, which include 60 free tunnel modes and 12 track modes on a rigid base [19].

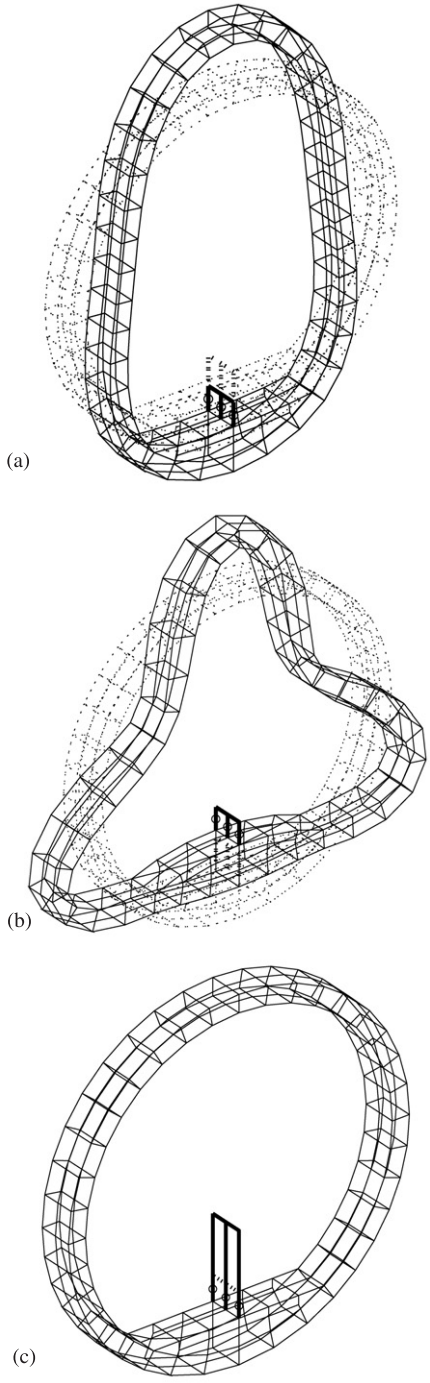

Fig. 7. (a,b) The free tunnel modes and quasi-static transmission into the track and (c) a track mode on a rigid base.

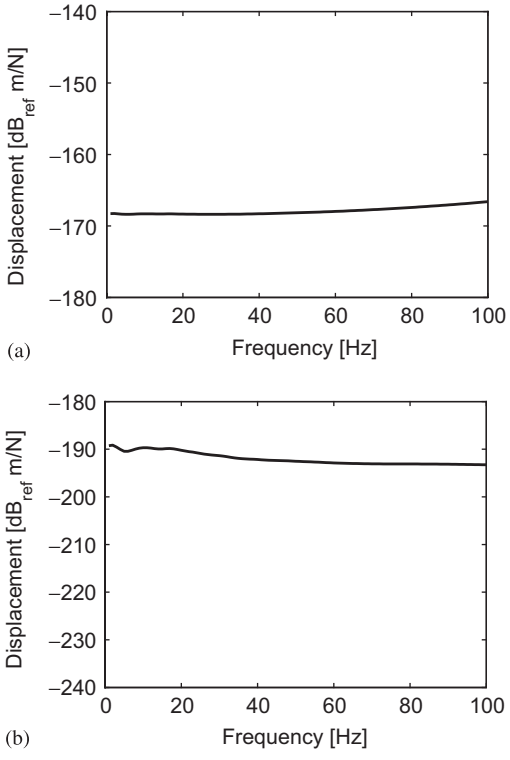

Fig. 8. Vertical transfer function at (a) the driving point on the rail $\{0\,\mathrm{m}, 0\,\mathrm{m}, -15.2\,\mathrm{m}\}^{\mathrm{T}}$ and (b) the tunnel invert $\{0\,\mathrm{m}, 0\,\mathrm{m}, -15.745\,\mathrm{m}\}^{\mathrm{T}}$.

Eq. (8) is solved to obtain the displacement field in the reference cell in the frequency–wavenumber domain. When the displacements $\tilde{\mathbf{u}}_t(\tilde{\mathbf{x}}, \kappa_y, \omega)$ and the stresses $\tilde{\mathbf{t}}_t(\tilde{\mathbf{x}}, \kappa_y, \omega)$ on the tunnel–soil interface are known, the wave field radiated into the soil is computed using the dynamic representation theorem in the unbounded layered soil domain in the reference cell. These soil displacements correspond to the transfer function in the frequency–wavenumber domain that are used in Eq. (5) to compute the incident wave field due to a moving train. The displacement field in the frequency domain at any point $\mathbf{x}$ is obtained after evaluation of the inverse Floquet transform.

Fig. 8 shows the track receptance and transfer function at the tunnel invert in the frequency domain. These transfer functions are defined as the response for a unit load applied on two rails. The response does not show any marked resonance of the tunnel, which is due to dynamic tunnel–soil interaction.

Fig. 9 shows the transfer function at $\{0\,\mathrm{m}, 0\,\mathrm{m}, 0\,\mathrm{m}\}^{\mathrm{T}}$ and $\{20\,\mathrm{m}, 0\,\mathrm{m}, 0\,\mathrm{m}\}^{\mathrm{T}}$ on the free surface. The response in the soil is characterized by undulating behavior which is due to the interference of the compression and shear or Rayleigh waves in the soil.

3.3. Axle loads

There are various excitation mechanisms responsible for generating vibrations due to moving trains. The excitation models developed under CONVURT [9,20] account for three mechanisms: the unevenness excitation due to wheel and rail roughness, the impact excitation due to rail joints and wheel flats, and the parametric excitation due to sleeper periodicity.

In this paper, the quasi-static excitation and the unevenness excitation due to wheel and rail roughness are considered. The parametric excitation is not taken into account as it would depend on the kind of a track installed in the tunnel, which is not yet decided for metro line 4. It has also been demonstrated by several authors [21–23] that the continuously supported model of the track is appropriate for the vertical track dynamics in most cases, apart from small modulation of the track stiffness at the sleeper passage frequency.

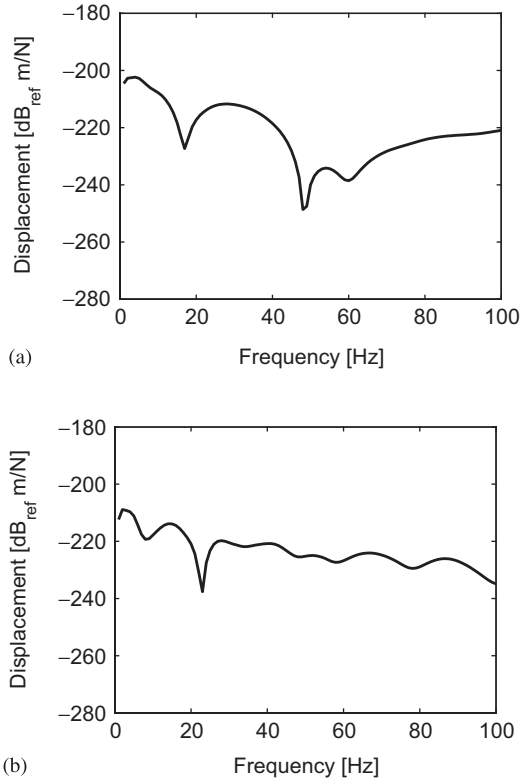

Fig. 9. Vertical transfer function at (a) $\{0\,\mathrm{m}, 0\,\mathrm{m}, 0\,\mathrm{m}\}^{\mathrm{T}}$ and (b) $\{20\,\mathrm{m}, 0\,\mathrm{m}, 0\,\mathrm{m}\}^{\mathrm{T}}$.

Moreover, as soft rail pads are considered, the variation of the receptance along the span is small and can be ignored.

The quasi-static excitation occurs when successive axles of the train pass over the track and can be modelled as constant forces moving along the track with train speed v. The time history $g_k(t)$ is equal to the total axle load P_k, which results from the dead weight of the train. The Fourier transform $\hat{g}_k(\omega)$ equals $2\pi P_k \delta(\omega)$.

Roughness is the main excitation source in the generation of vibrations from moving trains. For the simple case of vertical interaction between the wheel and the rail, the contact force $\hat{\mathbf{g}}(\omega)$ in the frequency domain, generated due to an uneven profile is computed from [24]:

$$[\hat{\mathbf{C}}^{v}(\omega) + \hat{\mathbf{C}}^{\mathrm{tr}}(\omega)]\hat{\mathbf{g}}(\omega) = \hat{\mathbf{u}}_{w/r}(\omega), \tag{9}$$

where $\hat{\mathbf{u}}_{w/r}(\omega)$ is the combined rail and wheel roughness, $\hat{\mathbf{C}}^{v}(\omega)$ is the compliance of the vehicle and $\hat{\mathbf{C}}^{\mathrm{tr}}(\omega)$ is the compliance of the track in the moving frame of reference.

The track compliance $\hat{\mathbf{C}}^{\mathrm{tr}}(\omega)$ can be computed in the fixed frame of reference, as the train speed is much less than the critical wave speed in the track–tunnel–soil system. For low train speeds, the element $C^{\mathrm{tr}}_{lk}(\omega)$ of the track compliance can be approximated as the response of the track at the position of axle l due to a unit load (static) at axle k. Fig. 8a shows a diagonal element of the track compliance computed from the coupled periodic FE–BE model.

The vehicle compliance is computed by modelling the rolling stock as a mass–spring–damper system. The rolling stock consists of coaches, bogies, axles and wheels, which are modelled as rigid bodies and are connected to each other by springs and dampers (Fig. 10). M_1, M_2, M_3, M_4 are the mass of the wheel tread, the wheel web and axle, the bogie, and the coach, respectively. K_1^* represents the stiffness of the resilient wheel. K_2 and K_3 are the stiffness of the primary and the secondary suspension, and C_2 and C_3 are the viscous damping factors of the primary and the secondary suspension.

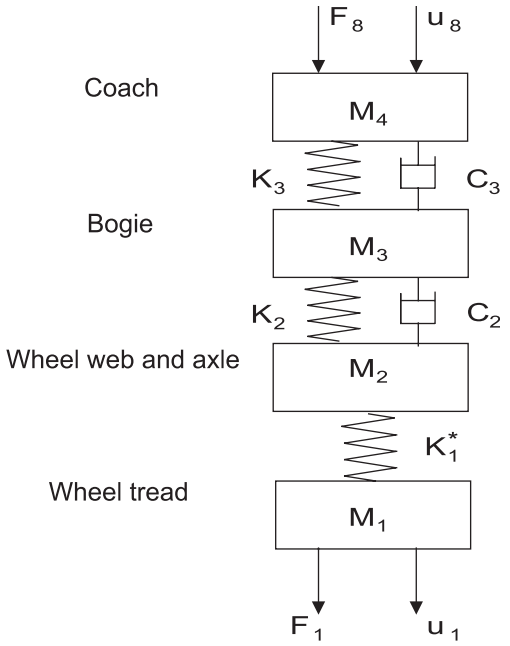

Fig. 10. Rolling stock decomposition into subsystems.

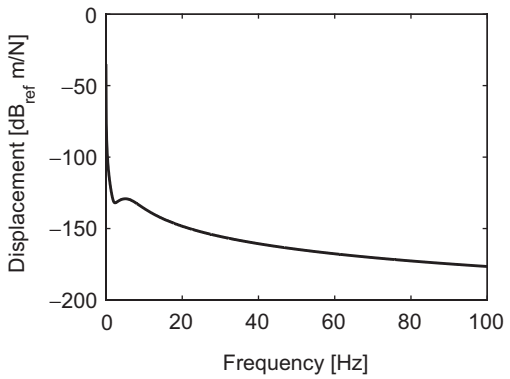

Fig. 11. Wheel receptance calculated from the rolling stock model.

The wheel receptance $\hat{C}^v$ at the contact point is equal to the displacement $\hat{u}_1$ for $\hat{F}_8 = 0$ and $\hat{F}_1 = 1$.

The rolling stock on metro line 4 will be VVVF style train consisting of 6 cars each of length 19 m. The bogie and axle distances on all cars are 12.6 and 2.3 m, respectively. The total mass of the train is 342 tons, resulting in an axle load of 139.8 kN. The mass of the coach with passengers is 43 tons, while the mass of the bogie and axle are 3.6 and 1.7 tons, respectively. The primary suspension has a stiffness $K_2 = 1.4 \times 10^6$ N/m and a damping $C_2 = 3 \times 10^4$ Ns/m. The secondary suspension has a stiffness $K_3 = 5.8 \times 10^5$ N/m and a damping $C_3 = 1.6 \times 10^5$ Ns/m. The speed of the train on metro line 4 is considered to be $v = 60$ km/h.

Fig. 11 shows the wheel receptance calculated for one wheel set. A peak appears at a low frequency that corresponds to the resonance of the coach on the bogie and can be approximately calculated as $1/(2\pi)\sqrt{K_3(1/M_3 + 1/M_4)} = 4.36$ Hz. Due to the high damping of the suspensions, the resonance of the bogie on the axle is not visible.

Table 2
Roughness parameter for FRA track classes

Track class	6	5	4	3	2	1
A' [10^{-7} m cycle]	1.06	1.69	2.96	5.29	9.52	16.72

The rail roughness $u_{w/r}(y)$ is modelled as a stochastic process characterized by a single-sided power spectral density (PSD) $\tilde{G}'_{w/r}(n_y)$, and can be written as a function of the cyclic wavenumber $n_y = f/v = 1/\lambda_y$ [25]:

$$\tilde{G}'_{w/r}(n_y) = \frac{A' n_{y2}^2 (n_y^2 + n_{y1}^2)}{n_y^4 (n_y^2 + n_{y2}^2)}. \tag{10}$$

Depending on the rail quality, the track is divided into six classes according to the Federal Railroad Administration (FRA), class 6 track being the best and class 1 the poorest. $n_{y1} = 0.0233$ cycle/m and $n_{y2} = 0.1312$ cycle/m are the break frequencies that do not change significantly for different track classes. The roughness parameter A' is strongly dependent on the track class and its values are summarized in Table 2.

The single-sided PSD $\tilde{G}_{w/r}(k_y)$ as a function of the wavenumber k_y is computed as $\tilde{G}_{w/r}(k_y) = \tilde{G}'_{w/r}(n_y)/(2\pi)$.

An artificial profile $u_{w/r}(y)$ is generated from the PSD-curve based on the superposition of simple random processes with known statistical properties. Let the single sided PSD $\tilde{G}_{w/r}(k_y)$ be defined in the interval $[k_{y1}, k_{y2}]$, where the range will depend on the frequencies of interest and the train speed. This interval is divided into N intervals with a width Δk_y and center wavenumber k_{yi}. An artificial profile $u_{w/r}(y)$ is generated [26] as the superposition of cosine functions with random phase angles θ_i in the interval $[0, 2\pi]$:

$$u_{w/r}(y) = \sum_{i=1}^{n} \alpha_i \cos(k_{yi} y - \theta_i). \tag{11}$$

The parameters α_i are determined by imposing that the mean square of the artificial profile is equal to the area under the PSD curve $\tilde{G}_{w/r}(k_y)$ in each interval Δk_{yi}, with center wavenumber k_{yi}. Hence,

$$\alpha_i = \sqrt{2 \tilde{G}_{w/r}(k_{yi}) \Delta k_y} \tag{12}$$

Fig. 12a shows the PSD of the rail unevenness for the FRA track classes 1 and 6. In the numerical example, FRA track class 1, corresponding to the poorest rail quality, is used for generating the artificial roughness profile $u_{w/r}(y)$. Fig. 12b shows the modulus of the rail roughness $\hat{u}_{w/r}(\omega)$ in the frequency domain obtained from the wavenumber representation of the roughness profile $\tilde{u}_{w/r}(k_y)$:

$$\hat{\mathbf{u}}_{w/r}(\omega) = \frac{1}{v} \tilde{u}_{w/r}\left(-\frac{\omega}{v}\right) \exp\left(\mathrm{i}\omega \frac{\mathbf{y}_a}{v}\right) \tag{13}$$

where the vector $\exp(\mathrm{i}\omega \mathbf{y}_a/v)$ accounts for the phase difference between the axles and is determined by the vector $\mathbf{y}_a$ that contains the initial position of all axles.

The dynamic axle loads are computed by accounting for the interaction between two rails and two wheels. Fig. 13 shows the dynamic wheel/rail interaction force $\hat{g}_k(\omega)$ at the front axle of the train as a function of the frequency, calculated from Eq. (9). The first peak appears at the anti-resonance frequency of the bogie mass on the primary and the secondary suspension. The second peak appears at the wheel–track resonance frequency around 61 Hz, which corresponds to the resonance of the unsprung mass of the rolling stock (wheel and axle) on the track stiffness.

3.4. Response during the passage of a train on metro line 4

After the computation of the excitation forces and the transfer functions in the frequency–wavenumber domain [19], the response to moving loads can be computed from Eq. (5) [27]. The response is calculated by adding the contribution of the dynamic forces and the quasi-static forces in the frequency domain.

Fig. 14 shows the frequency content and time history of the vertical velocity of the rail during the passage of the train at the speed of 60 km/h, which have been calculated accounting for both quasi-static as well

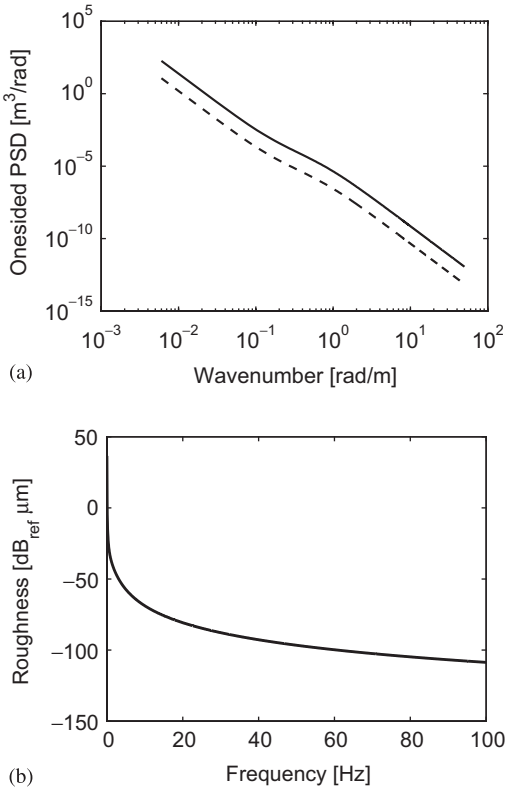

Fig. 12. (a) PSD curve of the rail unevenness according to FRA track classes 1 (solid line) and 6 (dashed line). (b) The magnitude of the rail roughness as a function of the frequency for FRA track class 1.

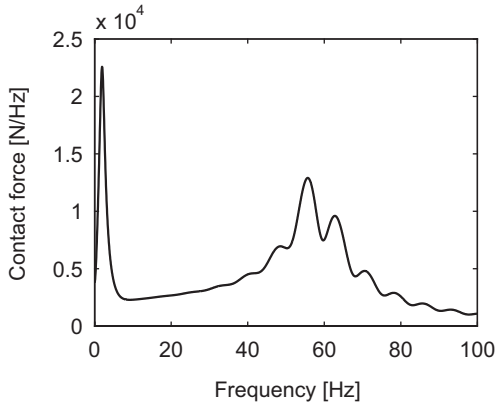

Fig. 13. Contact force due to the wheel–rail interaction.

unevenness excitation. Superimposed in Fig. 14a is the frequency content of the response due to the quasi-static loads (gray) only. It can be observed that quasi-static loads are more significant than the dynamic loads due to rail unevenness in the low-frequency range below 20 Hz. The spectrum is quasi-discrete due to the specific train composition. Fig. 14b enables the identification of the passage of the individual bogies.

The frequency content and time history of the vertical velocity on the tunnel invert is shown in Fig. 15. It can be seen that the maximum frequency content appears around the wheel–track resonance frequency of 61 Hz. The quasi-static effect is dominant at frequencies less than 5 Hz.

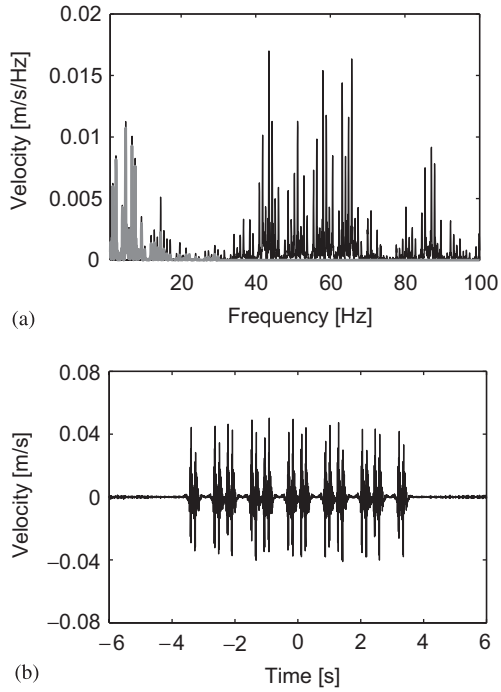

Fig. 14. (a) Frequency content and (b) time history of the vertical velocity of the rail. Superimposed on (a) is the frequency content of the vertical velocity due to the quasi-static loads (gray).

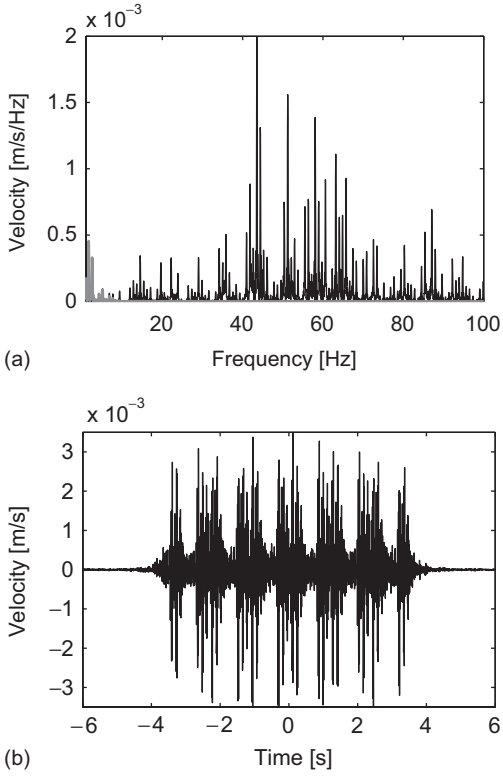

Fig. 15. (a) Frequency content and (b) time history of the vertical velocity of the tunnel invert. Superimposed on (a) is the frequency content of the vertical velocity due to the quasi-static loads (gray).

Fig. 16 shows the free-field velocity on the surface at $\{20\,\mathrm{m}, 0\,\mathrm{m}, 0\,\mathrm{m}\}^{\mathrm{T}}$. Again the dominant frequency content is around the wheel–track resonance frequency. The response in the free-field allows to observe the effect of the geometrical and the material damping in the soil. For a train speed ($v = 60\,\mathrm{km/h}$) lower than the wave velocities in the ground, the quasi-static excitation generates evanescent and leaky waves which decay importantly with distance [28]. It is clear from Fig. 16a that the contribution of the quasi-static loads is negligible and the dynamic loads due to the rail unevenness dominate the response.

Fig. 17a shows the one-third octave band RMS values of the vertical acceleration at $\{20\,\mathrm{m}, 0\,\mathrm{m}, 0\,\mathrm{m}\}^{\mathrm{T}}$. Superimposed on the same curve are the maximum allowable RMS values of the vertical acceleration for the Tecnai30 electron microscope. The RMS values of the predicted response enter zone III at frequencies below 6 Hz and at frequencies around the wheel–track resonance frequency. The vibrations at low frequencies are the consequence of the vehicle's suspension system. The existing background vibration levels due to road traffic outside the Physics Laboratory in channel CH1 are also shown in Fig. 17a. The measurement point CH1 is at a distance of about 17 m from the tunnel and is close to the point where results have been predicted. Subway induced vibrations are a matter of concern, as the response increases with respect to the background vibrations and enters zone III at low frequencies and around the wheel–track resonance frequency. However, it should be noted that the vibration levels at a distance of 20 m from the railway line are presented here, while the nearest wall of the laboratory is at a distance of 46 m from the railway line. Therefore, the vibrations near the Physics Laboratory are expected to be lower than the levels shown in Fig. 17a.

For a more relevant assessment of vibrations in the vicinity of the Physics Laboratory, the combined effect of the road and railway traffic is studied. Fig. 17b shows the one-third octave band RMS values of the vertical acceleration obtained after superposition of the measured vibrations from road traffic and the predicted vibrations from subways. The total vertical acceleration lies in zone II in the frequency range between 8 and 30 Hz due to the road traffic and it enters zone III in the frequency range below 6 Hz and around the wheel–track resonance frequency due to the railway traffic.

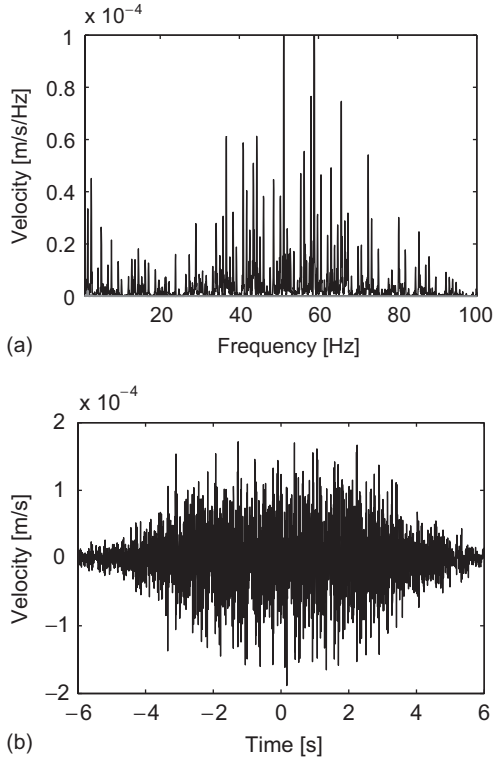

Fig. 16. (a) Frequency content and (b) time history of the vertical velocity at the point $\{20\,\mathrm{m}, 0\,\mathrm{m}, 0\,\mathrm{m}\}^{\mathrm{T}}$ on the free surface. Superimposed on (a) is the frequency content of the vertical velocity due to the quasi-static loads (gray).

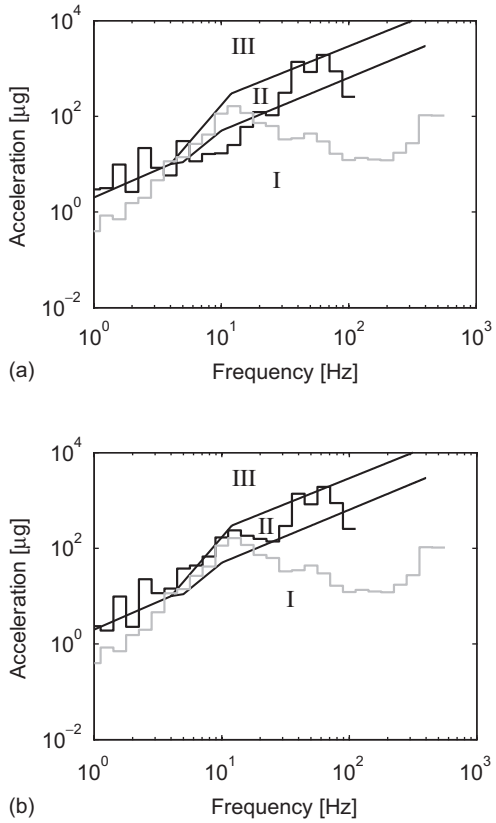

Fig. 17. One-third octave band RMS spectra of the vertical acceleration at $\{20\,\mathrm{m}, 0\,\mathrm{m}, 0\,\mathrm{m}\}^{\mathrm{T}}$ due to (a) only railway traffic (black) and (b) both railway and road traffic (black). Superimposed on the graphs are the spectrum of the background vibration levels due to road traffic (light gray) and the maximum allowable RMS values of the vertical acceleration for the Tecnai30 electron microscope.

4. Vibration measurements on line 1

To substantiate the previous numerical results, vibration measurements have also been performed on a site near line 1 of Beijing metro. The stretch of line 1 between Dongdan station and Jianguomen station is chosen for vibration measurements, as it has similar surroundings and soil stratification as the site north of Chengfulu station. The tunnels between Dongdan station and Jianguomen station are two parallel bored tunnels with a concrete lining embedded at a depth of 14.5 m in layers of fill material, silty clay, gravel and pebble. The two tunnels are under the Second Ring Road, which has heavy road traffic. In the following, the results of this measurement campaign are compared to the numerical predictions on line 4 of Beijing metro. It should be emphasized that the objective of this section is to only show that the predictions on metro line 4 are realistic and this comparison should not be regarded as the experimental validation of the numerical model.

The track inside the tunnel is a conventional non-ballasted concrete slab track, which has the same characteristics as the track considered on metro line 4. G-style and S-style trains are currently used on metro line 1, which have 6 carriages with a length of 19 m each and a total length of 116.6 m.

In situ vibration measurements on line 1 between the Dongdan and Jianguomen station have been performed to study the combined effect of road and railway traffic. Four channels are fixed at varying distance from the center line of the two tunnels to record the vibrations during the passage of the trains at varying speeds between 10 and 60 km/h.

Fig. 18a shows the one-third octave band RMS spectra of the vertical acceleration induced by vehicles on the road measured at 20, 40, 80 and 100 m from the tunnel. The dominant frequency content is between 10 and 30 Hz, which is the typical frequency range for road traffic induced vibrations. Fig. 18b shows similar results for another event, which has been recorded during the passage of the G-Style train at a speed of 30 km/h in

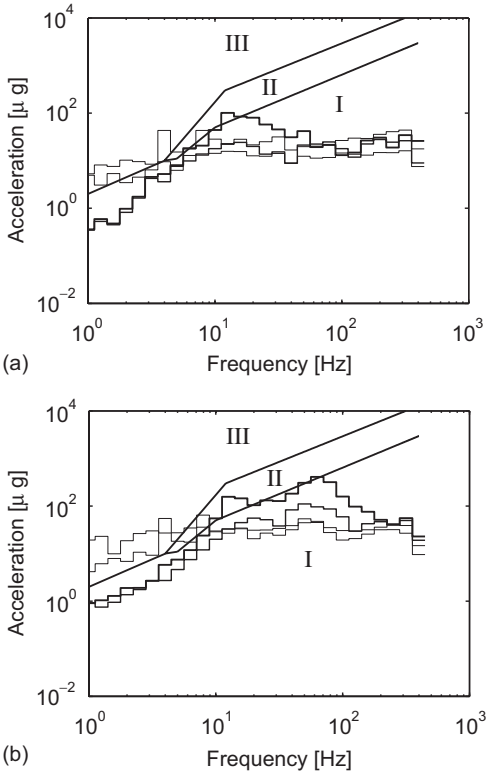

Fig. 18. One-third octave band RMS spectra of the vertical acceleration induced (a) by the road traffic only and (b) by the train (speed $v = 30$ km/h) and road traffic together at varying distances from the tunnel on metro line 1 (——— 20 m, ——— 40 m, ——— 80 m, ——— 100 m; decreasing line thickness). Superimposed on the graphs are the maximum allowable RMS values of the vertical acceleration for the Tecnai30 electron microscope.

addition to the traffic on the road. Comparison of these figures clearly shows the contribution of subway induced vibrations in the frequency range between 30 and 100 Hz. The measured accelerations show similar characteristics as the predictions on line 4 of Beijing metro.

Fig. 19 compares the RMS values of the background vibrations and the vibrations induced by cars, buses, the G-style train and the S-style train, measured at a distance of 27 and 80 m from the central line of the tunnels. These one-third octave band spectra are derived from the mean value of all recorded events. The contributions of the road traffic can be distinguished from that of the train in the tunnel. For the road traffic, the main contribution is in the lower frequency band between 10 and 30 Hz, while for the metro trains, the main contribution is in a wider frequency range between 10 and 100 Hz. The vibration levels induced by metro trains are of higher magnitude than the vibrations induced by the road traffic.

Fig. 20 shows the one-third octave band RMS spectra of the vertical acceleration at a distance of 20 m from the tunnel, during the passage of the G-style train at a speed of 50 km/h (in absence of road traffic). The figure also displays the predicted results at the same distance from the tunnel on metro line 4, north of Chengfulu station, for the poorest and the best quality rail according to the FRA track classes. In the frequency range between 8 and 100 Hz, the measured results on line 1 lie within the predicted results on line 4 for the FRA track classes 1 and 6. The measured and predicted results agree reasonably well, despite the fact that both sites are different. The different response at low frequencies can be attributed to different site characteristics and also to different types of trains running on both sections, as it is significantly influenced by the suspension system of the train. This comparison shows that the vibrations predicted on line 4 are realistic. The future operation of line 4 of Beijing metro will significantly contribute to vibrations around the wheel–track resonance frequency, where the vibration levels also enter into zones II and III. Therefore, it is desirable to consider a vibration countermeasure, which effectively mitigates these vibrations.

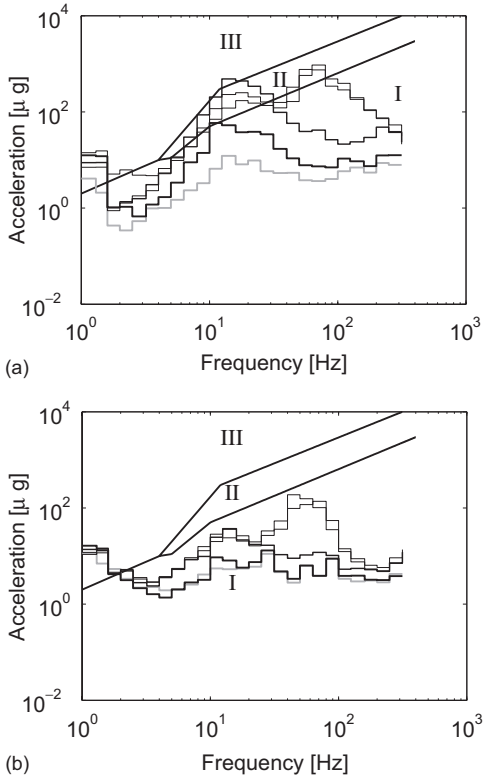

Fig. 19. RMS values of the background vibrations (gray) and the vibrations induced by traffic (—— cars, —— buses, —— G-style train, —— S-style train; decreasing line thickness) at a distance of (a) 27 m and (b) 80 m from the central line of the tunnels. Superimposed on the graphs are the maximum allowable RMS values of the vertical acceleration for the Tecnai30 electron microscope.

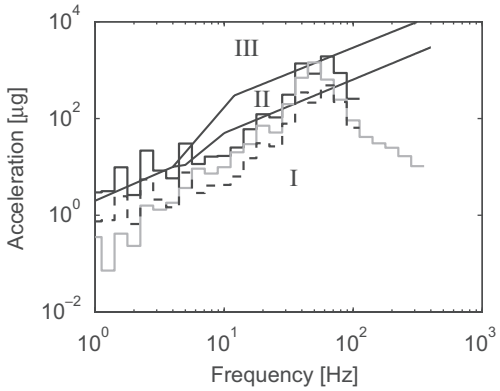

Fig. 20. One-third octave band RMS spectra of the vertical acceleration at a distance of 20 m from the tunnel measured on metro line 1 (gray) and predicted on metro line 4 (black) for the case of the FRA track classes 1 (solid line) and 6 (dashed line). Superimposed on the graph are the maximum allowable RMS values of the vertical acceleration for the Tecnai30 electron microscope.

5. Vibration mitigation using a floating slab track

Floating slab track is widely used as an effective measure of vibration isolation for underground tunnels. Rubber bearings or steel springs are accommodated between the slab and the tunnel bed. A floating track bed system has already been installed inside the test tunnel of Beijing Jiaotong University, where some preliminary

tests have been performed to determine the vibration isolation efficiency of the system. It consists of a concrete slab mounted on spring boxes. The isolation frequency of this floating slab track, which is defined as the resonance frequency of a single-degree-of-freedom system with a mass equal to the track's mass per unit length and stiffness equal to the vertical stiffness of the support, is about 8 Hz. A similar system with an isolation frequency of 7.9 Hz is planned to be installed in the tunnel north of Chengfulu station.

In this paper, the vibration isolation efficiency of a floating slab track with a resonance frequency of 7.9 Hz is investigated. Discontinuous concrete slabs of dimensions 31 m × 2.5 m × 0.45 m are supported by two rows of 17 springs with a spring stiffness of 6.9 MN/m each. The slab is modelled as a continuous beam coupled to the tunnel via a uniform support, that has a low stiffness corresponding to the isolation frequency of 7.9 Hz.

The track is efficiently incorporated in the model using Craig–Bampton substructuring [11], which avoids the recomputation of the soil impedance that only depends on the tunnel modes. This approach facilitates future parametric studies on the efficiency of different vibration isolation measures in the tunnel.

Figs. 21 and 22 show the frequency content and time history of the vertical velocity on the tunnel invert and the free surface for the case of the isolated track. Comparison with the unisolated case (Figs. 15 and 16) clearly demonstrates the efficiency of the floating slab track well above the isolation frequency 7.9 Hz. However, at low frequencies, there is an increase in the response which can deteriorate the existing situation. The floating slab track allows the vibrations to propagate along the slab before being transmitted to the tunnel and the soil, resulting in a reduced response in the free-field at frequencies higher than the isolation frequency [29].

Fig. 23 shows the one-third octave band RMS values of the vertical acceleration, obtained after superposition of the background vibration levels and the predicted vibrations from subways in the case of the isolated and the unisolated track. Above the isolation frequency, the vibration levels after isolating the track do not increase with respect to the existing vibrations due to road traffic. The isolation prevents the vibrations

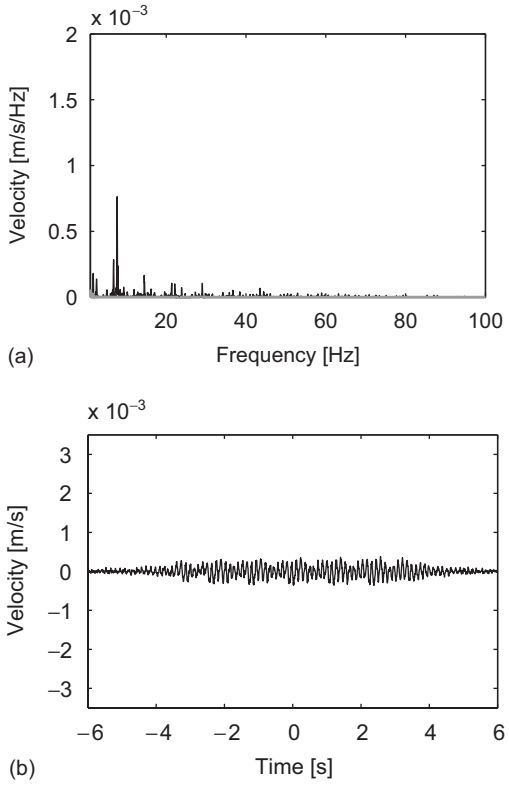

Fig. 21. (a) Frequency content and (b) time history of the vertical velocity of the tunnel invert, for the case of the isolated track.

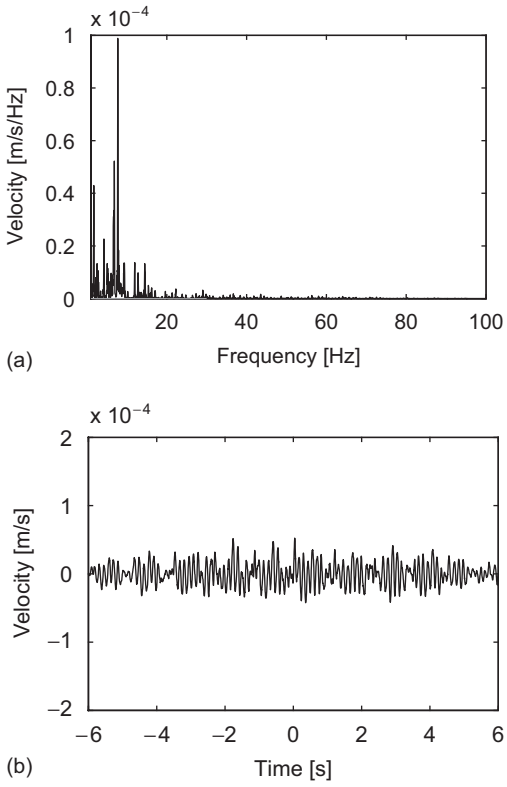

Fig. 22. (a) Frequency content and (b) time history of the vertical velocity at the point $\{20\,\mathrm{m}, 0\,\mathrm{m}, 0\,\mathrm{m}\}^{\mathrm{T}}$ on the free surface, for the case of the isolated track.

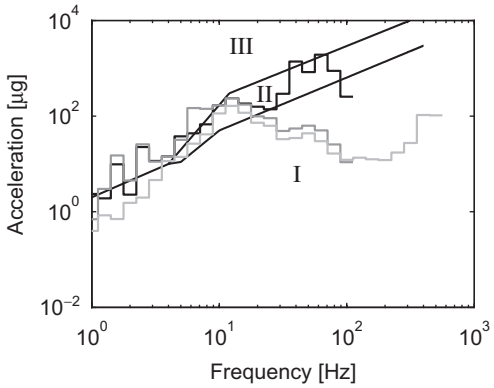

Fig. 23. One-third octave band RMS spectra of the vertical acceleration at $\{20\,\mathrm{m}, 0\,\mathrm{m}, 0\,\mathrm{m}\}^{\mathrm{T}}$ accounting for the vibrations due to road traffic and subway induced vibrations for the case of the unisolated (black) and the isolated (dark gray) track. Superimposed on the graph are the spectrum of existing background vibrations due to road traffic (light gray) and the maximum allowable RMS values of the vertical acceleration for the Tecnai30 electron microscope.

with frequency content around the wheel–track resonance to enter into zones II and III. The important contribution of the subway induced vibrations near the wheel–track resonance frequency [30] is effectively negated by installing a 7.9 Hz floating slab track. However, it should be noted that no benefit is achieved at lower frequencies by installing a 7.9 Hz floating slab track; the vibrations at low frequencies further increase and still lie in zone III.

6. Conclusions

The main objective of the work presented in the paper is to predict the free field vibration induced by trains on line 4 of Beijing metro in the proximity of the Physics Laboratory of Beijing University. Metro line 4 is currently under construction and the future operation of the line may adversely affect the performance of sensitive equipment inside the laboratory. The tunnel north of Chengfulu station on line 4 of Beijing metro is modelled using the coupled periodic FE–BE model and the response in the vicinity of the subway is computed.

For the numerical prediction, quasi-static excitation and unevenness excitation due to rail roughness are considered. The wheel–track interaction forces are first estimated, followed by the computation of the response in the free-field by solving a dynamic track–tunnel–soil interaction problem.

Vibration measurements have been performed on the site of the Physics Laboratory of Beijing University to determine the background vibration levels. The road traffic heavily influences the vibration levels outside and inside the Physics Laboratory. The dominant frequency range for road traffic induced vibrations is identified between 10 and 30 Hz. The combined effect of road and railway traffic is studied by superposing the predicted and measured vibrations.

In addition, vibration measurements have also been performed on line 1 of Beijing metro between Dongdan station and Jianguomen station. The effect of traffic and subway induced vibrations is analyzed. The road traffic contributes to the vibration levels in a narrow frequency band from 10 to 30 Hz, while the underground railways contribute to a wider range of frequencies from 10 to 100 Hz. It is observed that the magnitude of the vibrations induced by subways is higher than the road traffic. This site closely resembles the site north of Chengfulu station, and therefore the measured vibrations are compared to the predicted vibrations on metro line 4. The correspondence between the two results is good, which suggests that the predicted results are realistic.

The comparison of the one-third octave band spectra of the predicted and the measured results suggests that the vibrations generated from the metro trains might exceed the background vibration levels at frequencies between 20 and 100 Hz and at low frequencies below 6 Hz. The most important frequency for ground-borne vibrations is the wheel–track resonance frequency, which is usually between 40 and 100 Hz. This fact is also confirmed by the measurements performed on line 1 of Beijing metro. The efficiency of a 7.9 Hz floating slab track is demonstrated in the numerical example, which shows to be very effective in attenuating the disturbances well above the isolation frequency. However, it results in an increased response at the resonance frequency of the slab.

The paper demonstrates the applicability of the state-of-the-art three-dimensional coupled periodic FE–BE model in an engineering analysis to study the efficiency of a vibration countermeasure.

Acknowledgments

The results presented in this paper have been obtained within the frame of the Bilateral project BIL/04/17 ''Railway traffic induced vibrations in the environment''. The project is funded by the Research Council of K.U.Leuven and by the National Natural Science Foundation of China. Their financial support is gratefully acknowledged.

References

[1] K.H. Chua, T. Balendra, K.W. Lo, Groundborne vibrations due to trains in tunnels, *Earthquake Engineering and Structural Dynamics* 21 (5) (1992) 445–460.

[2] K.H. Chua, K.W. Lo, T. Balendra, Building response due to subway train traffic, *Journal of Geotechnical Engineering, Proceedings of the ASCE* 121 (11) (1995) 747–754.

[3] W. Rücker, S. Said, Erschütterungsübertragung zwischen U-Bahn-Tunneln und dicht benachbarten Gebäuden, Forschungsbericht 199, Bundesanstalt für Materialforschung und -prüfung, Berlin, 1994.

[4] M. Mohammadi, D.L. Karabalis, Dynamic 3-d soil–railway track interaction by BEM–FEM, *Earthquake Engineering and Structural Dynamics* 24 (1995) 1177–1193.

[5] O. von Estorff, M. Firuziaan, K. Friedrich, G. Pflanz, G. Schmid, A three-dimensional FEM/BEM model for the investigation of railway tracks, in: N. Chouw, G. Schmid (Eds.), *Proceedings of the International Workshop Wave 2000, Wave propagation, Moving load, Vibration reduction*, Ruhr University, Germany, A.A. Balkema, Rotterdam, December 2000, pp. 157–172.
[6] K. Abe, D. Satou, T. Suzuki, M. Furuta, Three-dimensional analysis of subway track vibrations due to running wheels, in: N. Chouw, G. Schmid (Eds.), *Proceedings of the International Workshop Wave 2000, Wave propagation, Moving load, Vibration reduction*, Ruhr University, Germany, A.A. Balkema, Rotterdam, December 2000, pp. 149–156.
[7] X. Sheng, C.J.C. Jones, D.J. Thompson, Prediction of ground vibration from trains using the wavenumber finite and boundary element methods, *Journal of Sound and Vibration* 293 (2006) 575–586.
[8] L. Andersen, C.J.C. Jones, Coupled boundary and finite element analysis of vibration from railway tunnels—a comparison of two- and three-dimensional models, *Journal of Sound and Vibration* 293 (2006) 611–625.
[9] ⟨http://www.convurt.com⟩, 2003.
[10] D. Clouteau, M. Arnst, T.M. Al-Hussaini, G. Degrande, Free field vibrations due to dynamic loading on a tunnel embedded in a stratified medium, *Journal of Sound and Vibration* 283 (1–2) (2005) 173–199.
[11] G. Degrande, D. Clouteau, R. Othman, M. Arnst, H. Chebli, R. Klein, P. Chatterjee, B. Janssens, A numerical model for ground-borne vibrations from underground railway traffic based on a periodic finite element—boundary element formulation, *Journal of Sound and Vibration* 293 (3–5) (2006) 645–666;
G. Degrande, D. Clouteau, R. Othman, M. Arnst, H. Chebli, R. Klein, P. Chatterjee, B. Janssens, *Proceedings of the 8th International Workshop on Railway Noise*, Buxton, UK, 8–11 September 2004.
[12] G. Lombaert, G. Degrande, D. Clouteau, Numerical modelling of free field traffic induced vibrations, *Soil Dynamics and Earthquake Engineering* 19 (7) (2000) 473–488.
[13] H. Chebli, O. Ramzi, D. Clouteau, Response of periodic structures due to moving loads, *Comptes Rendus Mécanique* 334 (2006) 347–352.
[14] S. Gupta, G. Degrande, H. Chebli, D. Clouteau, M.F.M. Hussein, H.E.M. Hunt, A coupled periodic fe-be model for ground-borne vibrations from underground railways, in: C.A. Mota Soares (Ed.), *Proceedings of the 3rd European Conference on Computational Mechanics*, Lisbon, Portugal, June 2006.
[15] D. Clouteau, M.L. Elhabre, D. Aubry, Periodic BEM and FEM–BEM coupling: application to seismic behaviour of very long structures, *Computational Mechanics* 25 (2000) 567–577.
[16] D. Clouteau, D. Aubry, M.L. Elhabre, E. Savin, Periodic and stochastic BEM for large structures embedded in an elastic half-space, in: M. Bonnet, A-M. Sändig, W.L. Wendland (Eds), *Mathematical Aspects of Boundary Element Methods*, CRC Press, London, 1999, pp. 91–102.
[17] M.L. Elhabre, Modélisation de l'interaction Sismique Sol-fluide-parois Moulées Suivant une Approche Périodique, PhD Thesis, Laboratoire de Mécanique des Sols, Structures et Matériaux, Ecole Centrale de Paris, 2000.
[18] R.J. Craig, M. Bampton, Coupling of substructures for dynamic analyses, *AIAA Journal* 6 (7) (1968) 1313–1319.
[19] W. Liu, S. Gupta, G. Degrande, W. Liu, Numerical modelling of vibrations induced by underground railway traffic on metro line 4 in Beijing, First Progress Report BWM-2006-08, Bilateral Project BIL/04/17, Department of Civil Engineering, K.U.Leuven, May 2006.
[20] J. Charlier, P. Bouvet, N. Vincent, Convurt Project. WP3: development of excitation model. Report REF.450.003.RA.02.A, CONVURT EC-Growth Project G3RD-CT-2000-00381, Vibratec, October 2002.
[21] A.V. Metrikine, A.V. Vostroukhov, Periodically supported beam on a visco-elastic layer as a model for dynamic analysis of a high-speed railway track, *International Journal of Solids and Structures* 40 (2003) 5723–5752.
[22] H. Takemiya, X. Bian, Substructure simulation of inhomogeneous track and layered ground dynamic interaction under train passage, *Journal of Engineering Mechanics* 131 (7) (2005) 699–711.
[23] X. Sheng, C.J.C. Jones, D.J. Thompson, Response of infinite periodic structures to moving or stationary harmonic loads, *Journal of Sound and Vibration* 282 (2005) 125–149.
[24] G. Lombaert, G. Degrande, J. Kogut, S. François, The experimental validation of a numerical model for the prediction of railway induced vibrations, *Journal of Sound and Vibration* 297 (3–5) (2006) 512–535.
[25] A. Hamid, T.L. Yang, Analytical description of track-geometry variations, *Transportation Research Record* 838 (1981) 19–26.
[26] C.Y. Yang, *Random Vibration of Structures*, Wiley, London, 1986.
[27] W. Liu, S. Gupta, G. Degrande, W. Liu, Numerical modelling of vibrations induced by underground railway traffic on metro line 4 in Beijing, Second Progress Report BWM-2006-11, Bilateral Project BIL/04/17, Department of Civil Engineering, K.U.Leuven, August 2006.
[28] X. Sheng, C.J.C. Jones, D.J. Thompson, A comparison of a theoretical model for quasi-statically and dynamically induced environmental vibration from trains with measurements, *Journal of Sound and Vibration* 267 (3) (2003) 621–635.
[29] G. Lombaert, G. Degrande, B. Vanhauwere, B. Vandeborght, S. François, The control of ground borne vibrations from railway traffic by means of continuous floating slabs, *Journal of Sound and Vibration* 297 (3–5) (2006) 946–961.
[30] M. Heckl, G. Hauck, R. Wettschureck, Structural-borne sound and vibration from rail traffic, *Journal of Sound and Vibration* 193 (1) (1996) 175–184.